Carbohydrate Polymers 208 (2019) 302–313

Contents lists available at ScienceDirect

Carbohydrate Polymers

journal homepage: www.elsevier.com/locate/carbpol

# Effects of the anti-angiogenic carbohydrate-peptide conjugate, chitooligosaccharide-ES2 on endothelial cells and tumor-bearing mice

Zhendong Wang[a,b], Yan Li[a,b], Liang Xing[c], Feng Sun[a,b], Zhifang Yang[a,b], Fengshan Wang[a,b,d], Haining Tan[a,b,d,*]

[a] National Glycoengineering Research Center, Shandong University, Jinan 250012, Shandong, PR China
[b] Shandong Provincial Key Laboratory of Carbohydrate Chemistry and Glycobiology, Shandong University, Jinan 250012, Shanong, PR China
[c] The Bureau of Science, Technology And Intellectual Property of Yantai Economic & Technical Development Zone, Yantai 264006, Shandong, PR China
[d] School of Pharmaceutical Sciences, Shandong University, Jinan 250012, Shandong, PR China

ARTICLE INFO

*Keywords:*
HTCOSC-ES2
Anti-angiogenic
Anti-tumor
Cellular uptake
Apoptosis and cycle

ABSTRACT

Most solid tumors require neovascularization during their growth. In our previous study, ES2 (IVRRADRAAVP) was covalently conjugated to soluble chitooligosaccharide chloride (HTCOSC) to form one novel HTCOSC-ES2 conjugate, which displayed better anti-angiogenic activity. In this work, the intracellular distribution and endocytosis of the conjugate in endothelial cells, as well effects on endothelial cell cycle and apoptosis were investigated. In addition, pharmacokinetic and antitumor studies were conducted. HTCOSC-ES2 entered the cell *via* clathrin and lipid valve pathway and was transported to the nucleus *via* lysosomal transport mechanism. Unlike ES2, HTCOSC-ES2 effectively inhibited the growth of endothelial cells and promoted apoptosis; thus, it could inhibit tumor angiogenesis, resulting in strong anti-tumor activity *in vivo*. The half-life of HTCOSC-ES2 was also prolonged, and its clearance was delayed. Immunohistochemistry assays showed that HTCOSC-ES2 obviously reduced the microvessel density, decreased the expression of VEGF, and increased the expression of caspase-3.

## 1. Introduction

With the development of anti-angiogenic agents, including proteins, peptides, carbohydrates, and small-molecule compounds, several potential antitumor drugs based on cutting off the nutritional supply of tumors have been developed (Folkman, 1972). Two effective drugs, endostatin and an 11-amino acid peptide derived from the *C*-terminus of endostatin (ES2, IVRRADRAAVP) displayed high bioactivity, poor stability and short half-life (Folkman, 2006a; Sun et al., 2018; Yu et al., 2016). However, owing to its simple structure, ES2 displayed better inhibition of angiogenesis, and its activity was approximately 3-fold higher than that of the complete ES sequence (Qiu et al., 2013; Tjin et al., 2005; Wickstrom, Alitalo, & Keski Oja, 2004).

In our previous study, we focused on the anti-angiogenic peptide, ES2, which was covalently conjugated to soluble *O*-(2-hydroxy) propyl-3-trimethyl ammonium chitooligosaccharide chloride (HTCOSC) to overcome its poor stability and low cell affinity. HTCOSC exhibits several favorable properties, such as non-toxicity, biocompatibility, blood compatibility, and biodegradability, making it widely used in the medical field (Liu, Xin, Liu, Zhang, & li, 2017; Yu et al., 2016). After conjugation, HTCOSC-ES2 showed improved stability and better anti-angiogenic activity both *in vitro* and *in vivo*. Besides these, HTCOSC-ES2 was supposed to arrest endothelial cells at $G_0/G_1$ stage and induce cell apoptosis more effectively, display longer half-life and better anti-tumor activity *in vivo*. Thus, the intracellular distribution and endocytosis of HTCOSC-ES2 in the endothelial cells, its effects on endothelial cell cycle and apoptosis, and its effects in tumor-bearing mice, as well as its half-life and tissue distribution *in vivo* were need to be studied. In this study, methyl thiazolyl tetrazolium (MTT) assay, laser confocal microscopy, flow cytometry, and *in vivo* pharmacokinetic and antitumor studies were carried out.

Vascular endothelial growth factor (VEGF) is one of the most important inducers of angiogenesis; therefore, it plays an important role in tumor angiogenesis (Gianni Barrera et al., 2012). Inhibition of VEGF expression could significantly inhibit tumor angiogenesis (Hosseini, Rajabibazl, Ebrahimizadeh, & Dehbidi, 2015). Therefore, the effects of HTCOSC-ES2 conjugate on VEGF expression were also investigated. Caspase-3 is a key molecule for apoptotic activation, where its expression has been shown to correlate with apoptosis (Ling et al., 2007). Therefore, the effects of HTCOSC-ES2 conjugate on caspase-3

* Corresponding author at: National Glycoengineering Research Center, Shandong University, Jinan 250012, Shandong, PR China.
*E-mail address:* hainingtan@sdu.edu.cn (H. Tan).

https://doi.org/10.1016/j.carbpol.2018.12.089
Received 25 October 2018; Received in revised form 19 December 2018; Accepted 27 December 2018
Available online 28 December 2018
0144-8617/ 

expression were examined. Immunohistochemistry is a simple, visual, and reliable method to determine the expression of VEGF and caspase-3 (Liu et al., 2015; Talib & Saleh, 2015). Microvessel density (MVD), an indicator of tumor angiogenesis, was also measured using immunohistochemistry (Ma et al., 2012; Shi et al., 2016). Thus, immunohistochemistry was employed to discuss the effects of HTCOSC-ES2 conjugate on VEGF, caspase-3 and MVD, and HTCOSC-ES2 was supposed to inhibit VEGF expression, MVD and up-regulate caspase-3 expression more effectively than ES2.

## 2. Experimental

### 2.1. Materials

ES2 purchased from China Pep-tides Co. Ltd (Shanghai, China). Chitosanoligosaccharide (average molecular weight 3000, deacetylation degree 85.85%, the average molecular weight is 3000, and molecular weight polydispersity index is 1.17) was purchased from Jinan Haidebei Marine Biological Engineering Co., Ltd. (Jinan, China). Fluorescein isothiocyanate (FITC), glycidyl trimethylammonium chloride (GTMAC), 1-ethyl-3-(3-dimethylaminopropyl) carbodiimide hydrochloride (EDC) and N-hydroxysulfosuccinimide sodium (NHS) were purchased from Sigma-Aldrich (St. Louis, MO, USA). The apoptosis kit was purchased from the Japan DOJINDO Laboratories (Japan). The cell cycle kit was purchased from Jiangsu KeyGEN BioTECH Co., Ltd. (Nanjing, China). Lyso-Tracker red and dialysis bags and 3-(4, 5-Dimethylthiazol-2-yl)-2, 5-diphenyltetrazolium bromide (MTT) were purchased from Beijing solarbio science & technology Co., Ltd. Hoechst 33,342 was purchased from Beyotime (Shanghai, China). Chlorpromazine was purchased from Shanghai Macklin Biochemical Co., Ltd. Methyl-β-cyclodextrin was purchased from Shanghai Yuanye Bio-Technology Co., Ltd. Nighty-six-well plates, 12-well plates, 6-well plates, 25 mL cell culture flasks and 15 mL centrifuge tubes were purchased from Corning INC (New York, USA). EA.hy926 endothelial cells (ATCC No.: CRL-2922) were obtained from the Shanghai Cell Bank of the Institute of Cell Biology, Chinese Academy of Sciences (Shanghai, China). All other chemicals and reagents were of the highest commercial grade available.

All C57BL/6 mice (4–6 weeks, 20 ± 2 g) were purchased from Jinan Pengyue Experimental Animal Breeding Co., Ltd. (Jinan, China), and raised under SPF conditions. All animal studies were approved by the Ethics Committee of Shandong University and conducted in accordance with laboratory animal care principles. Animal studies are reported in compliance with the ARRIVE guidelines.

### 2.2. Synthesis of HTCOSC and HTCOSC-ES2

HTCOSC and HTCOSC-ES2 were prepared and characterized as previously described (Yu et al., 2016). Brifely, purity of ES2 was determined using HPLC, the free amino group content of HTCOSC was determined by theninhydrin colorimetric method (Wan, Xu, Sun, & Li, 2013; Xu et al., 2016). ES2 (25 mg) was dissolved in phosphate buffer solution (PBS) (25 mL, pH 5.0, 10 mM), after EDC (80 mg) and NHS (20 mg) were added, the solution was stirred at room temperature for 30 min. HTCOSC (25 mg) was dissolved in PBS (25 mL, pH 8.0, 10 mM). Then, the HTCOSC (1.0 mg $mL^{-1}$) and an ES2 (1.0 mg $mL^{-1}$) were mixed at room temperature for 6–8 h. Finally, the obtained product was purified using a Sephadex G-25 column, and the phosphate (pH 6.0, 25 mM) eluent was collected, dialyzed, and lyophilized. The reaction was monitored using NMR, and the molecular weight of HTCOSC-ES2 was determined using MALDI-TOF-MS.

### 2.3. Characterization of ES2 and HTCOSC-ES2

The zeta potential and particle size were measured using the laser Doppler velocimetry mode of a Zeta Sizer Nano ZS-90 (Malvern Instruments Ltd, Worcestershire, UK). The zeta potential is pH dependent, the measurement was carried out at pH 7.2 (double distilled water). To characterize the morphology, ES2 and HTCOSC-ES2 were visualized with transmission electron microscopy. Each result was obtained from an average of at least 3 repetitions.

### 2.4. Cell proliferation assay

EAhy926 cells were cultured in DMEM medium (Hyclone) with 10% FBS and maintained under a 5% $CO_2$ atmosphere at 37 °C. The cells were seeded in 96-well plates ($5 \times 10^3$ cells · well $^{-1}$). After incubation overnight, endothelial cells were treated with ES2, ES2 & HTCOSC and HTCOSC-ES2 at peptide concentrations of 5, 25, 50, 75, 100, 125 μg $mL^{-1}$ for 48 h. Then, MTT reagent (20 μL) was added to each well and further cultured for 4 h under dark conditions. Afterwards, 150 μL dimethyl sulphoxide was added to each well to dissolve the formazan crystal after removing the medium. The absorbance was measured at 490 nm (Liang, Su, Liu, Wang, & Qi, 2015).

### 2.5. Intracellular distribution and endocytosis of ES2 and HTCOSC-ES2

First, fluorescein isothiocyanate (FITC) was used to mark ES2 and HTCOSC-ES2 (Ishimoto, Nemoto, Nagayoshi, Yamashita, & Hashida, 2006; Liu et al., 2009). FITC was dissolved in dimethyl sulfoxide (DMSO) at a concentration of 1 mg $mL^{-1}$. Then, it was added dropwise to ES2 or HTCOSC-ES2 while stirring at 25 °C for 2 h. Free fluorescein was removed, dialyzed, and lyophilized.

The cells were inoculated into a laser confocal dish ($15 \times 10^4$ cells · well $^{-1}$) and placed in a 5% $CO_2$ incubator at 37 °C for 16 h. Then, they were rinsed 3 times with phosphate-buffered saline (PBS) at 4 °C. FITC-HTCOSC-ES2 and FITC-ES2 were dissolved in a serum-free medium at a concentration of 125 μg $mL^{-1}$ and 1 mL was added to each dish. Then, they were incubated at 37 °C in a 5% $CO_2$ incubator for 0.5, 1, 2, and 3 h. After drug treatment, the medium was discarded, and cells were washed 3 times with PBS at 4 °C. The lysosomal red fluorescent probe was incubated for 15 min, and cells were washed 3 times with PBS at 4 °C. Hoechst 33,342 (5 μg $mL^{-1}$, 1 mL) was added, incubation was continued for 15 min, and the cells were washed 3 times with PBS at 4 °C. Then, PBS (200 μL) was added. The distribution of the drug in the cells was observed using a laser confocal microscope (Zeiss, LSM700, Germany) (Chen et al., 2011; Zhang, Yi, Zhang, Gulbins, & Li, 2006).

The cells were seeded into 12-well plates ($1 \times 10^5$ cells · $well^{-1}$) for 24 h. Then, they were incubated with the endocytic inhibitor, chlorpromazine (CPZ, 3 μg $mL^{-1}$) and methyl-β-cyclodextrin (1 μM) for 1 h at 37 °C in 5% $CO_2$. The cells were then treated with 125 μg $mL^{-1}$ FITC-ES2 and FITC-HTCOSC-ES2 (using ES2 as a standard) for 2 h. The cells were incubated with the same drug at the two concentrations in the absence of the inhibitor as controls. The cells were then placed in a flow cytometer (Beckman CytoFLEX FCM) to monitor the average fluorescence intensity within the cells (Chen et al., 2011).

### 2.6. Flow cytometry analysis of apoptosis

The cells were plated in 6-well plates at $3 \times 10^5$ cells · $well^{-1}$. After the cells adhered, they were starved overnight in serum-free Dulbecco's modified Eagle's medium (DMEM). Basic fibroblast growth factor (bFGF) solution (10 ng · $mL^{-1}$) was added to each well, including the blank wells and those containing different concentrations of the drugs (ES2: 5, 10, 25, and 50 mg $mL^{-1}$; HTCOSC-ES2: 5, 10, 25, and 50 mg $mL^{-1}$) (Chen et al., 2017). They were then incubated at 37 °C in the 5% $CO_2$ incubator for 24 h and collected by trypsin digestion (digestion time was not too long to avoid false positives). They were washed twice with PBS (1000 ×*g*, 3 min) at 4 °C. Finally, 300 μL of PBS was added to suspend the cells. Then, 5 μL of AnnexinV-FITC and 5 μL of PI were added, mixed, and allowed to react for 15 min at room temperature in the dark. Flow cytometry was used to detect DNA

content in apoptotic cells.

### 2.7. Anti-tumour actions of ES2 and HTCOSC-ES2

C57BL/6 female mice bearing B16F10 tumors were used to evaluate the therapeutic efficacy of ES2 and HTCOSC-ES2 on inhibition of tumour growth. The mice were subcutaneously injected at the right axillary space with 0.1 mL of cell suspension containing $1 \times 10^7$ cells. When the tumour tissue grew to 30–70 $mm^3$, the mice were randomly assigned to one of the three treatment groups (n = 4 for each group). The mice of each group were treated (iv.) every day with the different drugs as described in the following: normal saline, ES2 (20 mg $kg^{-1}$) and HTCOSC-ES2 (80 mg $kg^{-1}$) (Dhanabal et al., 1999; Jia et al., 2005; Pu et al., 2012).

All of the mice were treated for 14 days. The body weights was measured daily and tumor volumes was monitored by measuring the length and width of the tumor using a Vernier caliper (tumor size = length · $width^2$ · 0.5). At day 15, the mice were sacrificed and tumors from each group were surgically excised, rinsed with NS, wiped, weighed and photographed (Sun et al., 2018).

The mean tumor weight (MTW) in each group was obtained. The IR % of tumor weights was calculated by the following formula: IR (%) = $[1 - \mathrm{MTW}_{\text{treatment group}} \cdot \mathrm{MTW}^{-1}_{\text{control group}}] \times 100\%$.

### 2.8. Immunohistochemistry and imaging

Tumor tissues were collected, fixed, and sectioned for hematoxylin and eosin staining and immunohistochemical staining of CD31. According to the Weidner method (Weidner, 1995), the entire slice was scanned at low magnification to find three high-density regions (hot spots), and then the microvessels were counted at a magnification of 200× in these regions. The mean number of blood vessels was considered the MVD value (quantity · $HP^{-1}$) (Ding et al., 2017; He et al., 2017).

The slides were rinsed in PBS and incubated overnight at 4 °C with rabbit anti-mouse VEGF primary antibody (ABCAM, AB52917). Horseradish peroxidase-labeled goat anti-rabbit IgG (Servicebio, G23303) were used as secondary antibodies. After diaminobenzidine (DAB) color development, the nuclei were counterstained and dehydrated after sealing. Microscopic examination and analysis of the acquired images were performed, and images were captured at 200 × magnification. Image-Pro plus 6.0 software was used, and the integrated optical density (IOD) was determined.

The sections were placed in EDTA antigen retrieval buffer (pH 9) for antigen retrieval. After spontaneous fluorescence quenching and bovine serum albumin (BSA) blocking, the slides were washed with PBS and incubated overnight with rabbit anti-mouse caspase-3 primary antibody (Servicebio, GB11009) at 4 °C. Fluorescent labeled goat anti-rabbit CY3 (Servicebio, GB 21303) was used as a secondary antibody. Counterstaining of the nucleus was carried out using DAPI. The microscopic examination was carried out, and the immunofluorescence integrated optical density (IOD) was determined.

### 2.9. Pharmacokinetic study

ES2-FITC (1 mg) and HTCOSC-ES2-FITC (1 mg) were separately dissolved in 1 mL of blank plasma to obtain a 1 mg $mL^{-1}$ standard solution. Appropriate amounts were taken from the standard solution and diluted to 5, 10, 20, 50, 100, 200, 300, 400, 500 μg $mL^{-1}$ with blank plasma. Saturated 20% ammonium sulfate (AMS) (100 μL) was added to the diluted solution (100 μL), and the mixture was allowed to stand for 30 min at 4 °C. After centrifugation at 3000 × *g* for 10 min, the supernatant was discarded, 100 μL of double distilled water was used to dissolve the precipitate, and 20 μL of 0.1% sodium dodecyl sulfate (SDS) was added. The fluorescence intensity was plotted on the ordinate, and the serum concentration was plotted on the abscissa for linear regression.

ES2-FITC (1 mg) and HTCOSC-ES2-FITC (1 mg) were dissolved in 1 mL of the homogenate of each tissue to obtain a standard solution of 1 mg $mL^{-1}$. An appropriate volume was taken from the standard solution and diluted to 5, 10, 20, 50, 100, 200, 300, 400, 500 μg $mL^{-1}$ with the homogenate of each tissue. Trichloroacetic acid (TCA; 10%, 100 μL) was added to the diluted solution (100 μL), and precipitation was carried out at 4 °C for 30 min. After centrifugation at 3000 × *g* for 4 min at 4 °C, the supernatant was discarded, and 100 μL of double distilled water was added. The fluorescence intensity of each tube pellet was measured. The fluorescence intensity was plotted on the ordinate, and the standard concentration was plotted on the abscissa for linear regression.

C57BL/6 mice (*n* = 108, 50% males and 50% females) were subjected to starvation treatment for 24 h, and ES2-FITC (20 mg $kg^{-1}$) and HTCOSC-ES2-FITC (80 mg $kg^{-1}$) were injected intravenously. Immediately, 0.5, 1, 2, 4, 6, 8, 12, 24, and 36 h after injection, blood was collected. After centrifugation at 3000 × *g* for 10 min, 100 μL of the plasma and 20% saturated AMS were mixed, and allowed to stand for 30 min at 4 °C. After centrifugation at 3000 × *g* for 10 min, the supernatant was discarded, the residue was dissolved in 100 μL of double distilled water, and 100 μL of 0.1% SDS was added to measure the fluorescence intensity in each tube. The plasma concentration of ES2 and HTCOSC-ES2 at each time point was calculated from the standard curves, and the corresponding pharmacokinetic parameters were calculated (Mingming et al., 2017; Zhao et al., 2017).

After the blood was collected from the eyeballs, the heart, liver, spleen, lungs, and kidneys of the mice were isolated, washed in normal saline and dried using gauze. The tissues were weighed and cut into small pieces. Then, tissue lysates were prepared. After centrifugation at 3000 × *g* for 4 min at 4 °C, the supernatant was collected, 10% TCA (100 μL) was added, and precipitation was carried out at 4 °C for 30 min. After centrifugation at 3000 × *g* for 4 min at 4 °C, the supernatant was discarded, and 100 μL of double distilled water was added. The fluorescence intensity in each tube was measured (He et al., 2005; Li et al., 2015b).

### 2.10. Statistical analysis

Statistical analysis was performed using SPSS 19.0 (SPSS, USA) software. Calculate the standard deviation (SD) and average of each variable (data is mean ± SD). One-way analysis of variance (ANOVA) and two-way analysis of variance were used in GraphPad Prism 6, respectively. $P < 0.05$ indicates statistically significant difference.

## 3. Results

### 3.1. Characterization of ES2 and HTCOSC-ES2

As previously reported, the molecular weight of ES2, HTCOSC and HTCOSC-ES2 was 1223.45, 3000 and 4233.39, respectively. One molecular of soluble chitooligosaccharide HTCOSC was successfully conjugated to one molecular of ES2, through the amido bond between C-terminal carboxyl of ES2 andC-2-$NH_2$ of HTCOSC (Fig. 1A), and the HTCOSC-ES2 conjugate is stable. The zeta potentials of ES2 and HTCOSC-ES2 were determined to be 11.78 ± 1.84 and 22.3 ± 4.109 mv, respectively (Fig. 1B). HTCOSC-ES2 could form particles in solution because of the hydrophilic carbohydrate and the hydrophobic amino acids. According to the amino acids sequence ES2 and the results of transmission electron microscopy experiments, ES2 could also finally forms a micelle-like globular structure having a hydrophilic amino acid distributed outside and a hydrophobic amino acid distributed inside. The particle sizes of ES2 and HTCOSC-ES2 were 82.347 ± 1.904 and 243.5 ± 9.969 nm, respectively, which were similar to the results of transmission electron microscopy (Fig. 1C).

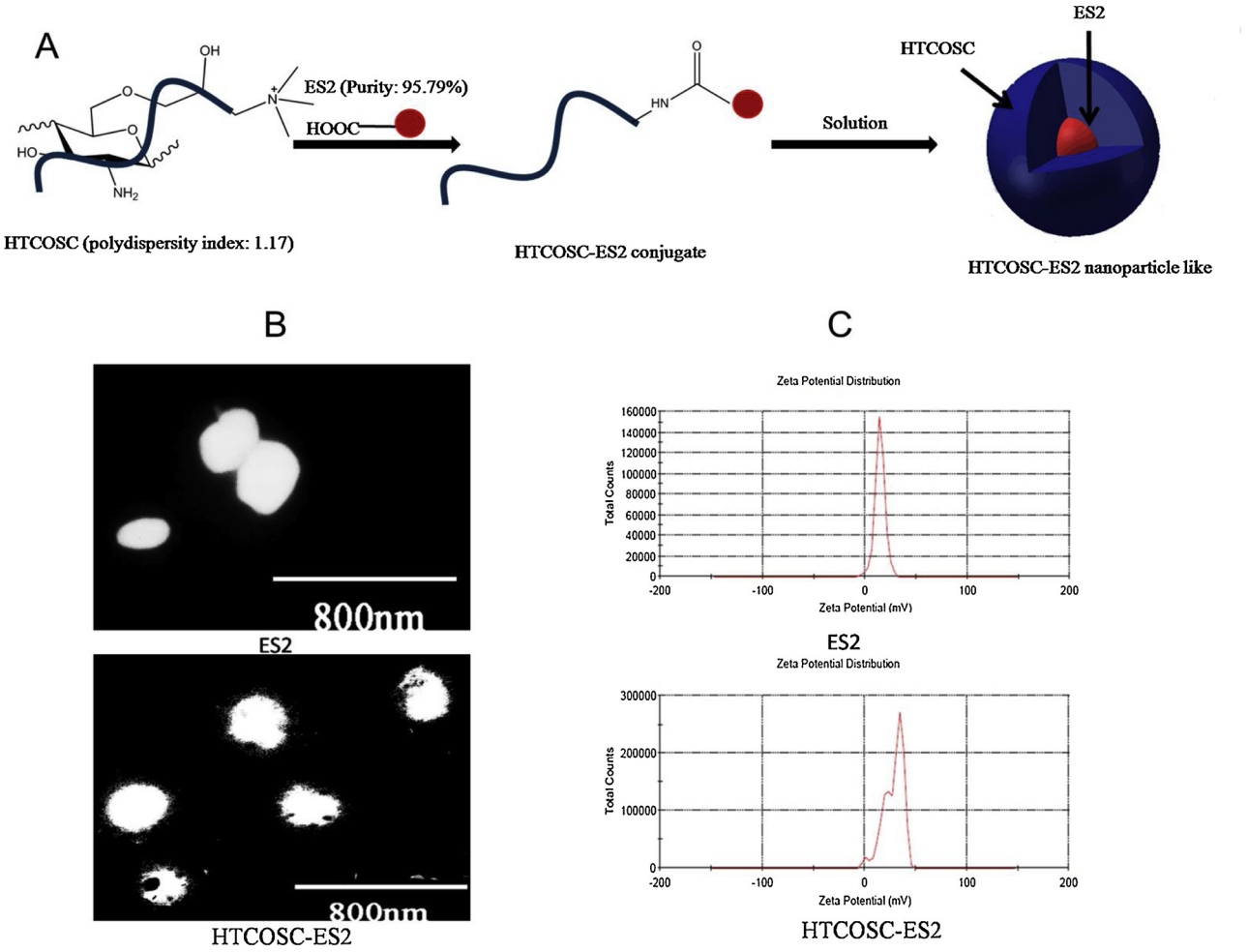


**Fig. 1.** Schematic illustration and physicochemical properties of the ES2 and HTCOSC-ES2. A: Schematic illustration; B: Transmission electron microscopy imaging; C: Zeta Potential.

### 3.2. Cell proliferation assay

As shown in Fig. 2, ES2, HTCOSC-ES2, and the mixture (HTCOSC and ES2) significantly inhibited endothelial cell proliferation at a concentration range from 5 to 125 μg mL$^{-1}$. As the concentration of ES2 increased, the inhibition rate also increased. HTCOSC-ES2 showed the strongest inhibitory activity at all concentrations tested, compared to the mixture and ES2.

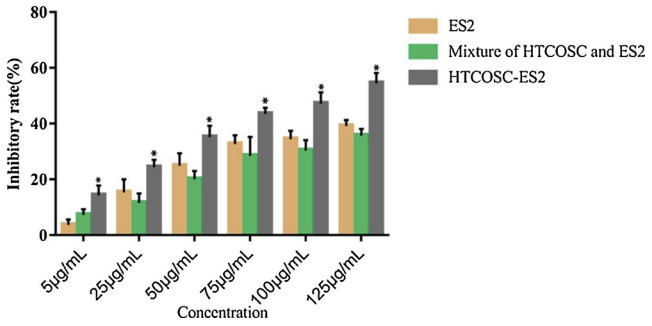


**Fig. 2.** ES2 and HTCOSC-ES2 inhibited endothelial cell proliferation *in vitro*. Data represent the mean ± standard deviation (SD), $n = 6$. * $p < 0.05$, compared to the ES2 or mixture groups.

### 3.3. Intracellular distribution and endocytosis of ES2 and HTCOSC-ES2

After incubation of the cells in the drug-containing medium for 0.5, 1, 2, and 3 h, green fluorescence (indicative of drug distribution) was mainly localized in a specific region inside the cells (Fig. 3A, B). However, after incubation of the cells in a medium containing the same concentration of FITC for 0.5, 1, 2, and 3 h, the fluorescence distribution was more dispersed (Fig. 3C).

After incubation of the cells in medium containing ES2-FITC and HTCOSC-ES2-FITC, the sub-cellular localization of the two drugs was similar (Fig. 3A, B). The green fluorescent signal of the drug overlapped with the red fluorescent signal of the lysosomes and the blue fluorescent signal of the nucleus. Results showed that after the cells absorbed ES2 and HTCOSC-ES2, they could be transported through the lysosomal pathway and finally entered the nucleus. HTCOSC-ES2 entered the cells after 1 h, whereas ES2 entered the cells after 0.5 h. The time to enter the cells of HTCOSC-ES2 was significantly prolonged.

Therefore, we further studied the involvement of the endocytic mechanism in endothelial cell uptake of ES2 and HTCOSC-ES2. CPZ inhibits clathrin-mediated endocytosis (Wang, Rothberg, & Anderson, 1993), whereas, methyl-β-cyclodextrin can disrupt endostatin-induced lipid raft aggregation (Jin, Zhang, Yi, & Li, 2008; Zhang et al., 2006). As shown in Fig. 3E, CPZ exhibited a slightly better inhibitory effect than β-cyclodextrin, indicating that ES2 predominantly entered endothelial cells through the clathrin pathway. However, the conjugate entered the endothelial cells primarily through the clathrin and lipid valve pathways (Fig. 3D). It was shown that the conjugate entered the cell mainly

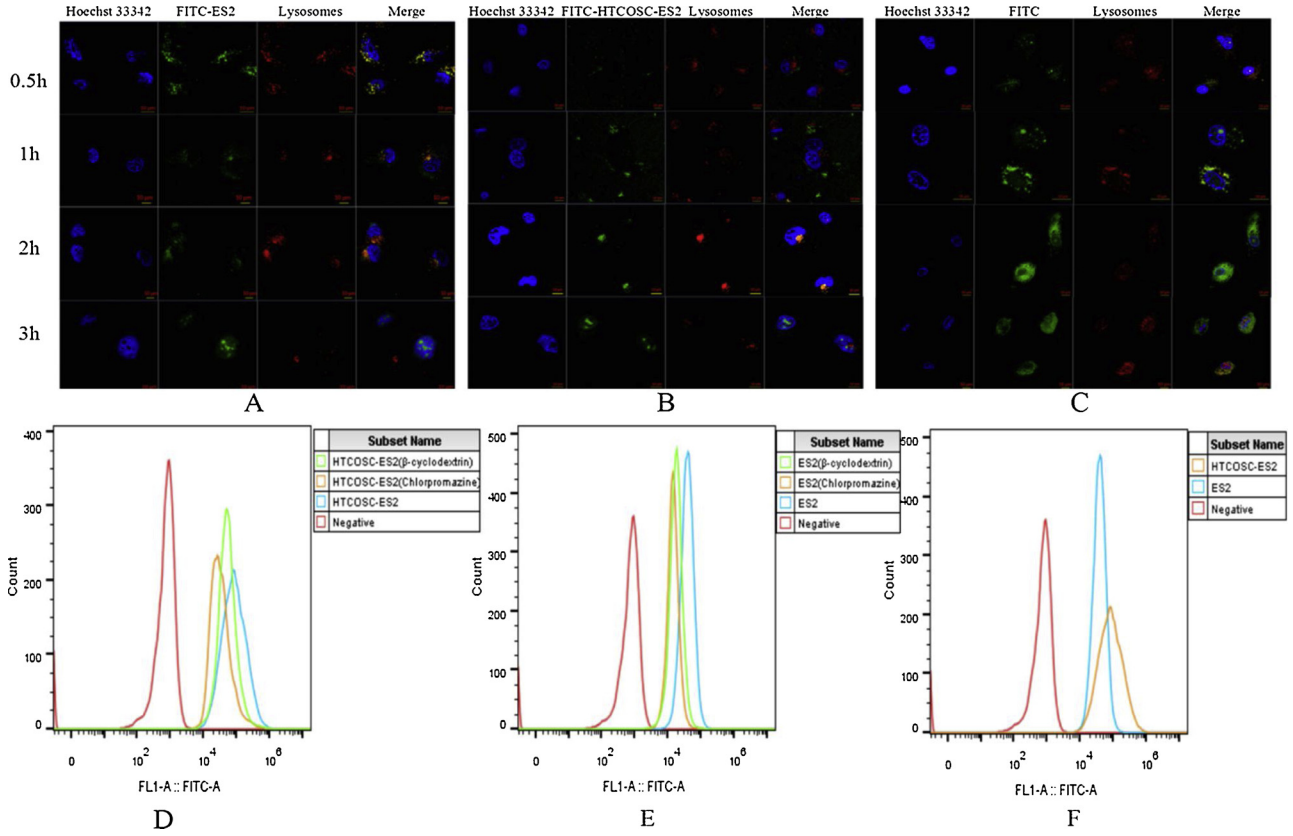


**Fig. 3.** A: Distribution of ES2 in endothelial cells, B: Distribution of HTCOSC-ES2 in endothelial cells, C: Distribution of FITC in endothelial cells, D: Flow cytometry of HTCOSC-ES2 after inhibitor treatment, E: Flow cytometry of ES2 after inhibitor treatment, F: Flow cytometry of untreated ES2 and HTCOSC-ES2.

through the clathrin pathway. When no inhibitor was added, the conjugate and ES2 completely entered the endothelial cells and were active for 2 h (Fig. 3F). These results are consistent with those of the cell distribution experiment. Therefore, the clathrin and lipid-valve pathways were suggested to mediate endothelial cell uptake of ES2 and HTCOSC-ES2, with the clathrin pathway being more important.

### 3.4. Flow cytometry analysis of apoptosis

Fig. 4 shows the results of flow cytometry analysis of apoptosis after endothelial cells were treated with different concentrations of ES2, HTCOSC-ES2, and the mixture. As the concentration of ES2 and HTCOSC-ES2 increased, the apoptotic rate of endothelial cells increased. Apoptosis of endothelial cells in the mixture and HTCOSC-ES2 groups was dose-dependent; however, apoptosis of endothelial cells was significant in the HTCOSC-ES2 group. These results indicated that both the high-concentration mixture and HTCOSC-ES2 could promote endothelial cell apoptosis, compared to the control group. Additionally, compared with ES2, HTCOSC-ES2 induced apoptosis of endothelial cells *in vitro* and increased the apoptotic rate of endothelial cells within a certain concentration range (Fig. 4B).

In this experiment, bFGF was used to promote proliferation of serum-activated endothelial cells and inhibit apoptosis of endothelial cells induced by growth factor deprivation (Karsan et al., 1997), because bFGF could induce the expression of antiapoptotic proteins, such as Bcl-2 (O'Connor et al., 2000), and overexpression of Bcl-2 could prevent serum and growth factor deprivation-induced apoptosis in endothelial cells (Karsan et al., 1997).

### 3.5. Cell cycle analysis

It has been reported that hypertrophic scar fibroblasts treated with rhEndostatin significantly accumulate in the $G_0/G_1$ phase and decrease in the S phase (Gong et al., 2016). At the molecular level, endostatin has been shown to downregulate the mRNA and protein expression of cyclin D1 by decreasing the phosphorylation of the Rb gene product, resulting in endothelial cell arrest in the $G_1$ phase. In addition, endostatin has been shown to reduce the stability of β-catenin, promote the degradation of β-catenin, inhibit Wnt signaling pathway, and inhibit endothelial cell migration, leading to endothelial cell arrest in the $G_1$ phase (Li et al., 2012). Cyclin D1 protein levels in human umbilical endothelial cells (HUVECs) increased by bFGF treatment, whereas bFGF-induced upregulation was inhibited by endostatin (Hanai et al., 2002). In this experiment, we found that the proportion of cells in the $G_1$ phase in the ES2, mixture, and HTCOSC-ES2 groups significantly increased, and the ratio of cells in the S and $G_2$ phases decreased, compared to those in the control group (Fig. 5), indicating that at a certain concentration, addition of ES2, similar to endostatin, could cause most of the endothelial cells to stay in the $G_1$ phase. In addition, the proportion of cells in the $G_1$ phase in the mixture group increased with the addition of HTCOSC, and the ratio of cells in the S and $G_2$/M phases decreased, compared to those in the ES2 group.

### 3.6. Antitumor activity of ES2 and HTCOSC-ES2

The *in vitro* experiments showed that ES2 and HTCOSC-ES2 not only inhibited the growth of endothelial cells by inhibiting the $G_1$ phase, but also promoted apoptosis of endothelial cells. Therefore, to investigate the effects of ES2 and HTCOSC-ES2 *in vivo*, C57 mice were injected with melanoma B16F10 cells to produce mice with melanoma xenografts. Then, ES2 (20 mg $kg^{-1}$) and HTCOSC-ES2 (80 mg $kg^{-1}$) were injected into the tail vein. The weight and volume of tumors in ES2- and HTCOSC-ES2-treated mice were significantly reduced, compared to those in the NaCl group (Fig. 6A, B), and the inhibition rates were 35.31

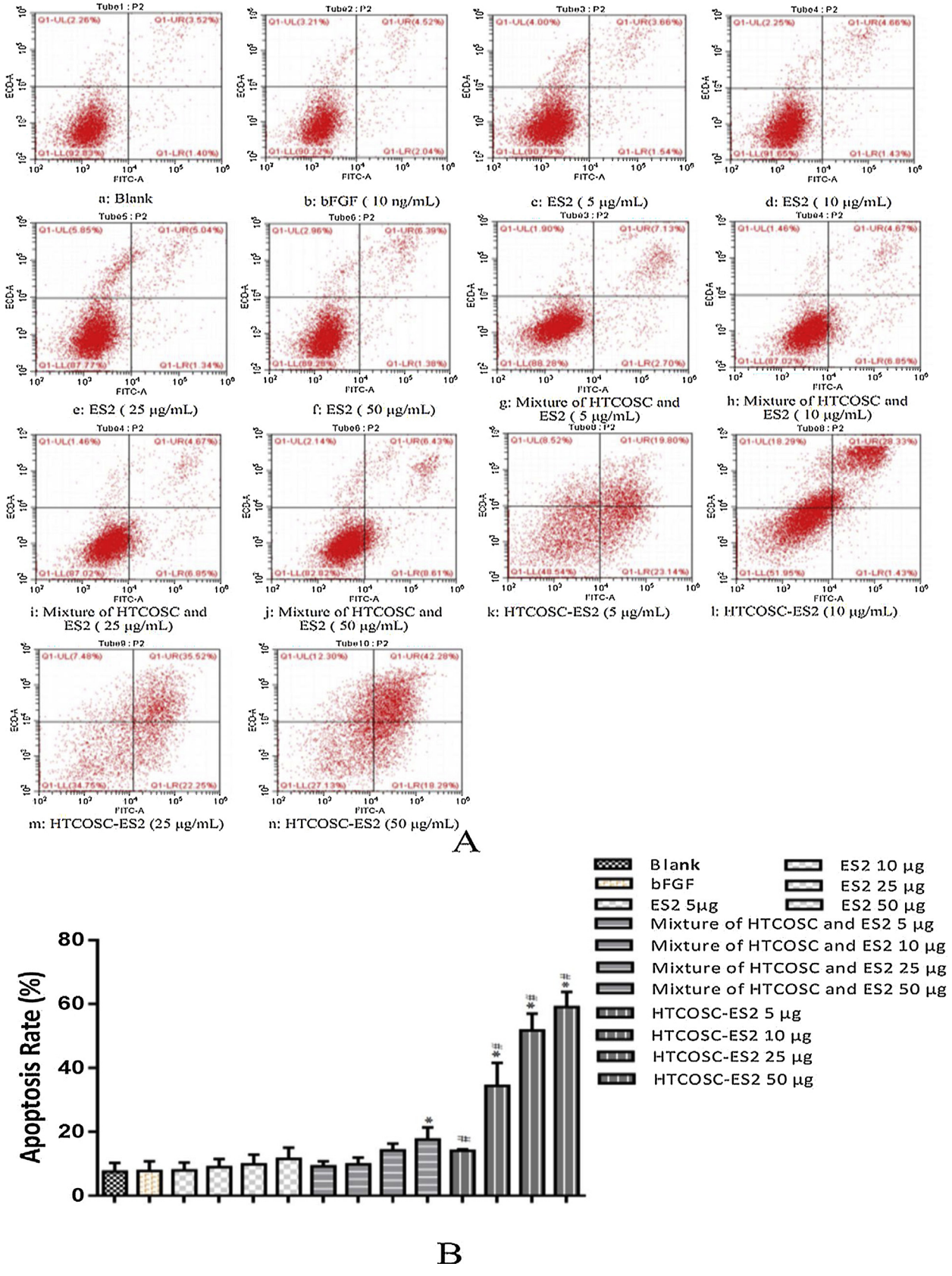


**Fig. 4.** A: Annexin V/PI shows apoptosis in EAhy926 endothelial cells. Flow cytometry (a) control, (b) bFGF alone, (c) ES2 5 μg $mL^{-1}$ and bFGF, (d) ES2 10 μg $mL^{-1}$ and bFGF, (e) ES2 25 μg $mL^{-1}$ and bFGF, (f) ES2 50 μg $mL^{-1}$ and bFGF, (g) Mixture of HTCOSC and ES2 (5 μg $mL^{-1}$) and bFGF, (h) Mixture of HTCOSC and ES2 (10 μg $mL^{-1}$) and bFGF, (i) Mixture of HTCOSC and ES2 (25 μg $mL^{-1}$) and bFGF, (j) Mixture of HTCOSC and ES2 (50 μg $mL^{-1}$) and bFGF, (k) HTCOSC-ES2 (5 μg $mL^{-1}$) and bFGF, (l) HTCOSC-ES2 (10 μg $mL^{-1}$) and bFGF, (m) HTCOSC-ES2 (25 μg $mL^{-1}$) and bFGF, (n) HTCOSC-ES2 (50 μg $mL^{-1}$) and bFGF. B: The percentage of apoptotic cells in all groups. The experiment was repeated 3 times (mean ± SD). $^{*}p < 0.05$ compared to the control group; $^{\#}p < 0.05$ compared to the ES2 group.

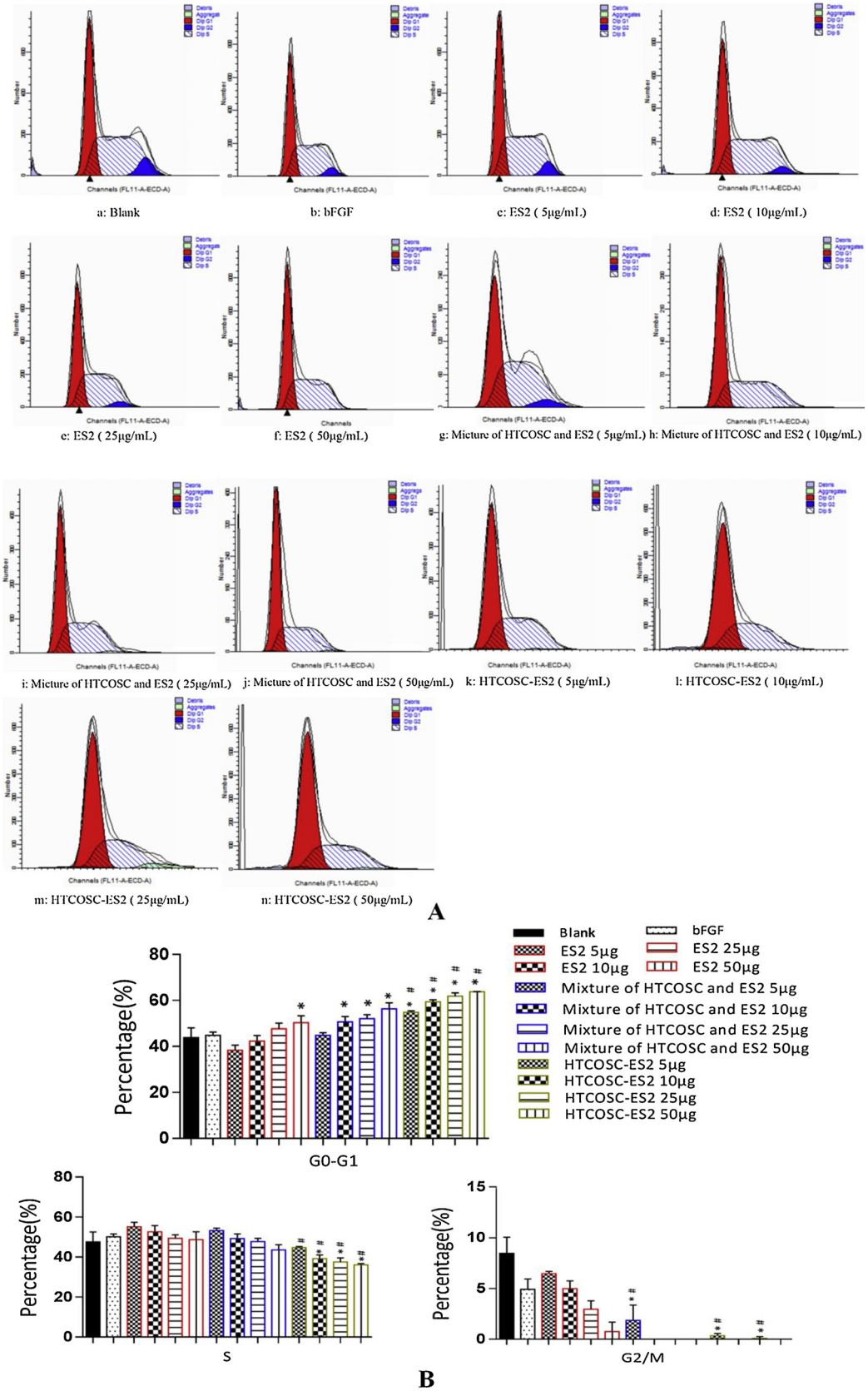


**Fig. 5.** A: Cell cycle diagrammonium sulfate of the control, ES2, mixture, and HTCOSC-ES2 groups at different concentrations. B: The histogram shows the proportions of cells in the $G_1$ phases of the cell cycle in different groups. The experiment was repeated 3 times (mean ± SD). $^{*}p < 0.05$ compared to the control group; $^{\#}p < 0.05$ compared to the ES2 group.

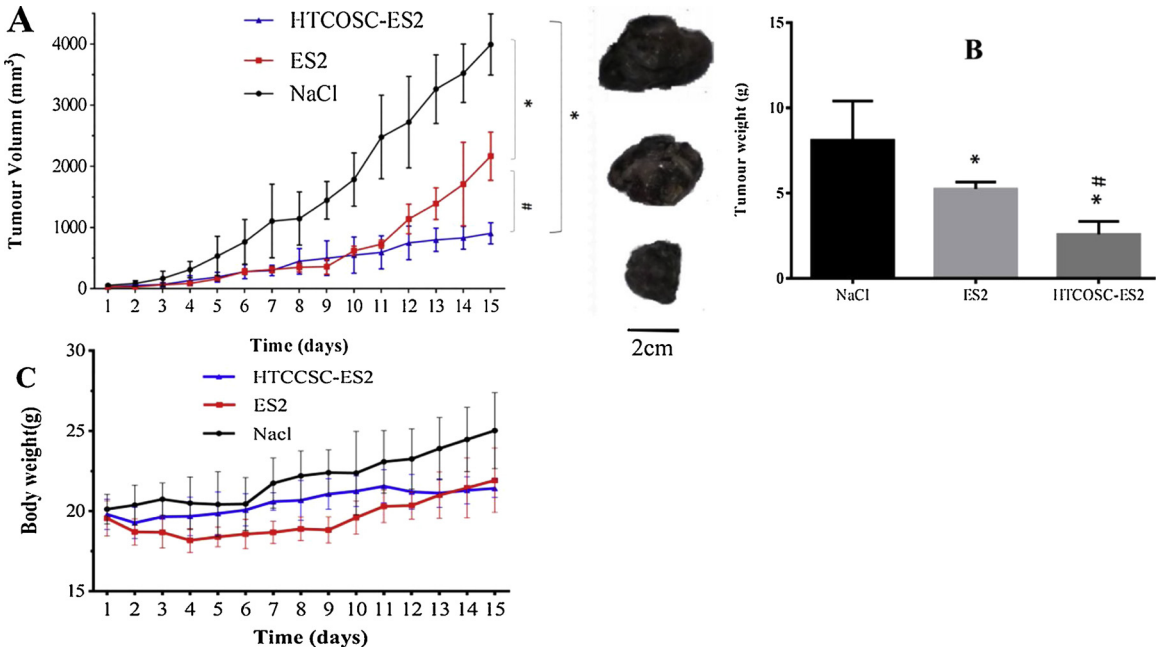


**Fig. 6.** ES2 and HTCOSC-ES2 inhibited the growth of mouse melanoma (mean ± SD, $n = 4$). A: Tumor volume in mice from different groups. B: Body weight of mice from different groups. C: Tumor weight in mice from different groups. $^{*}p < 0.05$ compared to the NaCl group; $^{\#}p < 0.05$ compared to the ES2 group.

and 68.21%, respectively.

### 3.7. Immunohistochemistry and imaging

VEGF is one of most important inducers of angiogenesis; therefore, it plays an important role in tumor angiogenesis (Makinen et al., 2001). Results of immunohistochemistry showed that VEGF was mainly localized in the cytoplasm and was expressed in all three groups (Fig. 7A). Furthermore, results showed that the expression of VEGF in the saline group was particularly high, compared to that in the other groups (Fig. 7D).

Vascular proliferation in tumor tissue reflects the ability of the tumor to induce angiogenesis; therefore, MVD can be used as an indicator of tumor angiogenesis (Deliu et al., 2016). The endothelial cell marker, CD31 is a novel microvascular marker that can be used to identify vascular endothelial cells and quantitatively assess their function. MVD and CD31 expression significantly decreased in the ES2 and HTCOSC-ES2 groups, compared to that in the saline group (Fig. 7D).

Fig. 6C shows the results of immunohistochemical analysis of apoptosis-related protein expression. Caspase-3 expression was significantly low in the saline group, compared to that in the other two groups, whereas it was significantly elevated in the HTCOSC-ES2 group (Fig. 7D).

### 3.8. Pharmacokinetic study

In this experiment, drugs were administered once into the tail vein. Fluorescence intensity at different time points was measured using a fluorescence microplate reader and used to calculate the corresponding concentration of ES2 or HTCOSC-ES2 (Mingming et al., 2017; Zhao et al., 2017). The concentration-time curve obtained is shown in Fig. 8. After single administration into the tail vein, the pharmacokinetic behavior of ES2 and HTCOSC-ES2 in mice was consistent with the two-compartment model.

Data were analyzed using DAS 2.0 software (Table 1). The half-life and maximum plasma concentration of HTCOSC-ES2 in the peripheral blood of mice were higher than those of ES2. In addition, the plasma concentration of ES2 decreased rapidly within 2 h. The area under the concentration-time curve of HTCOSC-ES2 was higher than that of ES2, whereas the plasma clearance rate was lower.

Drug concentrations in the heart, liver, spleen, lungs, and kidneys were measured after injection of ES2 and HTCOSC-ES2. As shown in Fig. 9, ES2 and HTCOSC-ES2 were mainly localized in the liver and kidneys. In the liver, both ES2 and HTCOSC-ES2 reached their maximum concentration at 2 h. However, HTCOSC-ES2 concentration in the liver was higher than that of ES2, indicating that HTCOSC-ES2 was more likely to enter the liver and exhibited liver targeting. In addition, HTCOSC-ES2 was distributed to the lungs, whereas its concentration in other tissues was very low. These results indicated that HTCOSC-ES2 exhibited greater liver targeting than ES2 (Li et al., 2015a, He et al., 2005; Li et al., 2015b).

## 4. Discussion

To improve the stability and prolong the short half-life of ES2, we combined HTCOSC with good safety, biocompatibility, and degradability with ES2, however, our previous studies did not investigate the distribution and endocytosis of ES2 and the conjugate into the endothelial cells, their effects on endothelial cell cycle and apoptosis, and their effects on half-life and tissue distribution *in vivo*. In this study, laser confocal microscopy showed that ES2 and HTCOSC-ES2 could be transported to the nucleus *via* the lysosomal pathway after uptake by the endothelial cells. HTCOSC-ES2 entered the cells after 1 h, whereas ES2 entered the cells after 0.5 h. The time for HTCOSC-ES2 to enter the cell was significantly extended. This could be explained as in the process of specific internalization of endostatin into the endothelial cells, caveolae/lipid and clathrin-coated depressions are associated with endostatin internalization (Chen et al., 2011). In addition, when the coating is formed, the curvature of the plasma membrane is driven by proteins with the BAR (Bin/amphiphysin/Rvs) domain (Farsad et al., 2001; Takei, Slepnev, Haucke, & De Camilli, 1999). However, the crystal structure of human Bin1/amphiphysin BAR consists of a crescent-shaped dimer structure and a positively charged concave surface (Casal et al., 2006). Therefore, we suggested that ES2 and ES might have the same cellular uptake mechanism, and since HTCOSC-ES2 contains a positive charge, the curvature might be affected, which could also affect the formation of the coated pit. We then further studied the uptake of ES2 and HTCOSC-ES2 by endothelial cells. We found that ES2

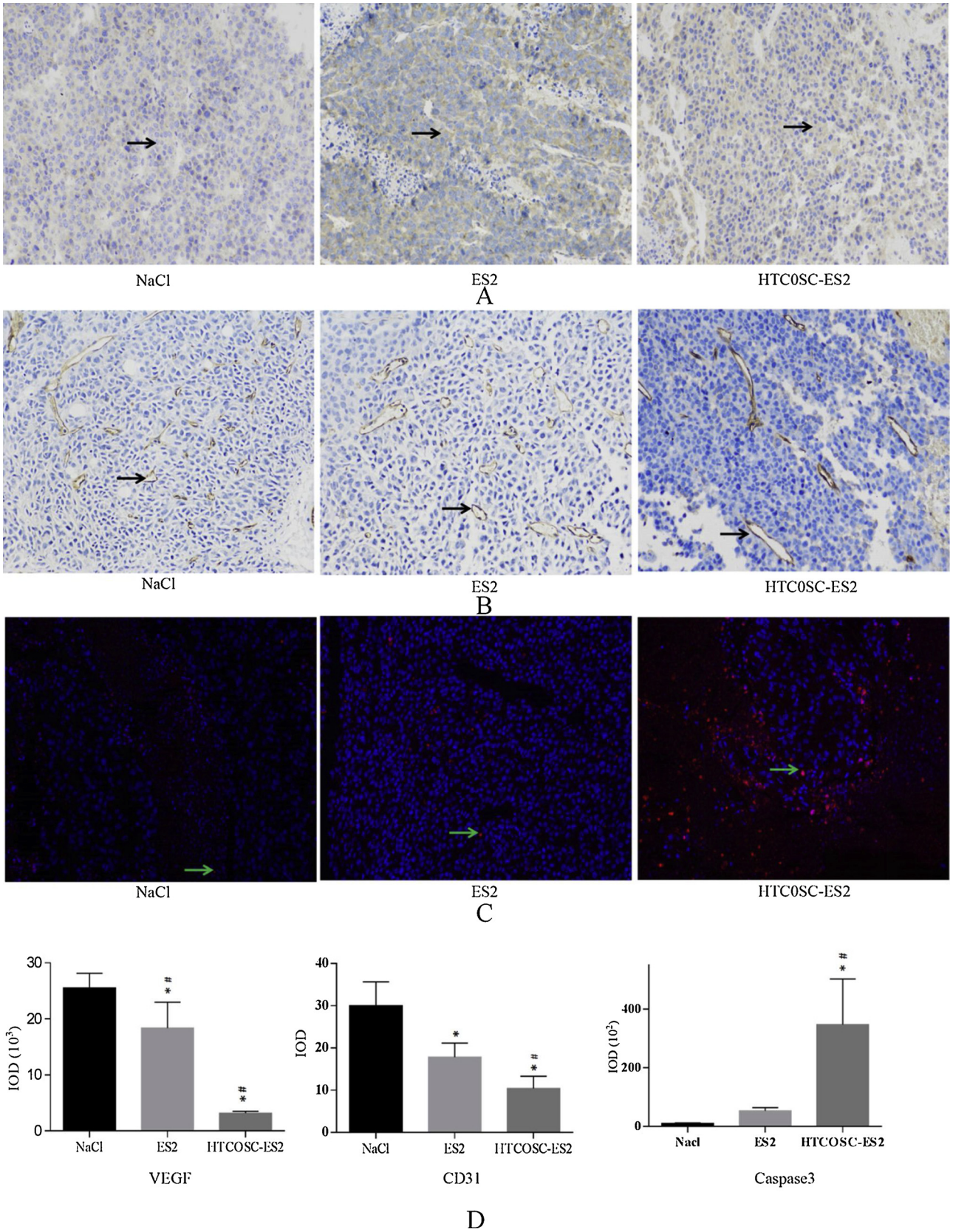


**Fig. 7.** A: Tumor sections (VEGF 200 ×) were immunohistochemically stained after treatment of tumor-bearing C57 mice with ES2 and HTCOSC-ES2. Yellow to brown stained cytoplasm indicates VEGF expression. Arrows shows tumor cells with stained cytoplasm. B: Immunohistochemical staining of tumor sections (MVD 200 ×) after treatment of tumor-bearing C57 mice with ES2 and HTCOSC-ES2. Positive immunohistochemical staining of CD31 was shown as the brown part in each figure. C: Immunofluorescence staining of tumor sections (caspase-3 200 ×) after treatment of tumor-bearing C57 mice with ES2 and HTCOSC-ES2. The red cytoplasm indicates the expression of caspase-3. The arrow indicates stained cytoplasm of tumor cells. D: The histogram shows the IOD values of VEGF, CD31, and caspase-3 in different groups. $^{*}p < 0.05$ compared to the control group; $^{\#}p < 0.05$ compared to the ES2 group.

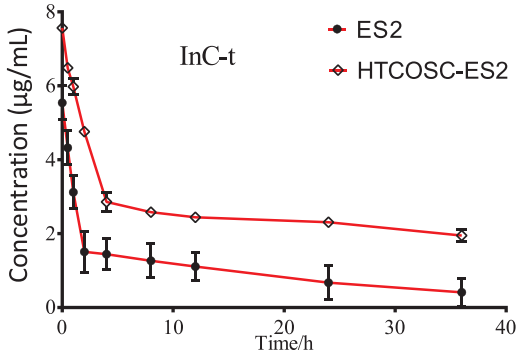


**Fig. 8.** Drug concentration-time curves after injection of ES2 and HTCOSC-ES2 into the tail vein of mice.

**Table 1**
The Pharmacokinetic parameters of ES2 and HTCOSC-ES2 in mice (i.v.).

| Parameters | ES2 | HTCOSC-ES2 |
|---|---|---|
| $t_{1/2}$(h) | 18.04 ± 2.38 | 29.17 ± 3.91 |
| AUC(μg/L*h) | 226.67 ± 95.20 | 1650.98 ± 129.41 |
| CL(L/h/kg) | 90.26 ± 39.94 | 10.32 ± 0.89 |
| $C_0$(μg/L) | 277.83 ± 121.86 | 1931.81 ± 75.35 |

Abbreviations: $t_{1/2}$half-life of ES2 and HTCOSC-ES2 in plasma; CLthe apparent volume of drug removed from the body per unit time; $C_0$plasma concentration at 0 h; AUCarea under the plasma concentration *versus* time curves of ES2-AF and HA-ES2-AF. The results are expressed as the means ± SD ($n$ = 6).

entered endothelial cells primarily *via* the clathrin pathway, whereas HTCOSC-ES2 entered the cells *via* both the clathrin and lipid valve pathways, where the clathrin pathway was also predominant.

Caspases belong to the family of cysteine proteases, and they play important roles in activation and induction of apoptosis. Caspases are involved in a cascade of actions triggered by proapoptotic signals that ultimately lead to cell apoptosis (Enari et al., 1998; Liu et al., 2017). In particular, caspase-3 is a key molecule for apoptotic activation (Enari et al., 1998). Studies have shown that endostatin-induced apoptosis depends on the activation of the mitochondrial apoptotic pathway, rather than the death receptor-mediated pathway, where endostatin can activate caspase-3 and induce apoptosis in HUVECs (Ling et al., 2009). Chitooligosaccharide induced apoptosis of hepatoma cells by increasing the expression of caspase-3 (Liu et al., 2017). Therefore, we hypothesized that HTCOSC-ES2 might also increase the expression of caspase-3, leading to cell apoptosis. As the concentration of ES2 and HTCOSC-ES2 increased, the apoptotic rate of endothelial cells increased. Unlike the ES2 group, apoptosis of endothelial cells in the mixture and HTCOSC-ES2 groups was dose-dependent, and apoptosis of endothelial cells in the HTCOSC-ES2 group was significantly different. These results showed that high-concentration mixture and HTCOSC-ES2 could promote endothelial cell apoptosis. HTCOSC-ES2 induced endothelial cell apoptosis *in vitro* and increased apoptotic rate of endothelial cells at a certain concentration range.

In terms of inhibition of endothelial cell proliferation, addition of ES2, similar to endostatin, forced most endothelial cells to remain in the $G_1$ phase. The proportion of cells in the $G_1$ phase increased in the mixture group, whereas the ratio of cells in the S and $G_2$/M phases decreased, compared to those in the ES2 group. Studies have shown that chitooligosaccharide can downregulate the expression of cyclin D1 in A549 cells and inhibit the proliferation of tumor cells (Li, Xing, Liu, & Li, 2016). In the HTCOSC-ES2 group, the proportion of cells in the $G_1$ phase significantly increased, whereas the proportion of cells in the S and $G_2$/M phases significantly decreased. In conclusion, ES2 was similar to endostatin, and chitooligosaccharide can downregulate the expression of cyclin D1. Therefore, conjugation of HTCOSC to ES2 enhanced its ability to inhibit cell proliferation.

HTCOSC-ES2 showed good proapoptotic effects and cell proliferation inhibitory activity *in vitro*. In the *in vivo* antitumor study, we found that the weight and volume of tumors in ES2- and HTCOSC-ES2-treated mice significantly decreased, compared to those in the NaCl group, with inhibition rates of 35.31 and 68.21%, respectively. However, studies have shown that the tumor inhibition rate is 50–60 % at endostatin dose of 10 mg · (kg · d)$^{-1}$(Dhanabal et al., 1999; Li et al., 2015a). Therefore, the therapeutic effect of HTCOSC-ES2 (20 mg kg$^{-1}$) is equivalent to that of endostatin (10 mg kg$^{-1}$).

Immunohistochemistry is a method to display histochemical components using specific antibodies to determine the expression of usually a protein or peptide (Inamura, 2018). Immunohistochemistry has the advantages of high sensitivity, specificity, accuracy, and speed, which greatly improves the accuracy of tumor pathological and differential diagnosis (approximately 50–70 %) (Ong, Jin, Jayasooriah, & Sinniah, 1996). Immunohistochemistry can be used to measure cell proliferation and apoptosis by detecting related protein expression. Currently, common targets are VEGF, MMP, p53, caspase-3, and CD31. For example, immunohistochemistry was used to evaluate the expression of VEGF and p53 in degenerated intervertebral disc tissue (Lu et al., 2013). Immunological expression of MMP-2, MMP-9 and CD31/MVD in oral squamous cell carcinoma was also previously assessed (Monteiro Amado et al., 2013). Immunostaining of caspase-3 was used to detect apoptosis of early circumventricular organ (CVO) after experimental subarachnoid hemorrhage (SAH) in rats (Edebali et al., 2014).

The role of endostatin in tumor angiogenesis has been confirmed (Ling et al., 2007). In view of the current reports that ES2 inhibits blood vessel formation and tumor growth *in vivo*, this study investigated the

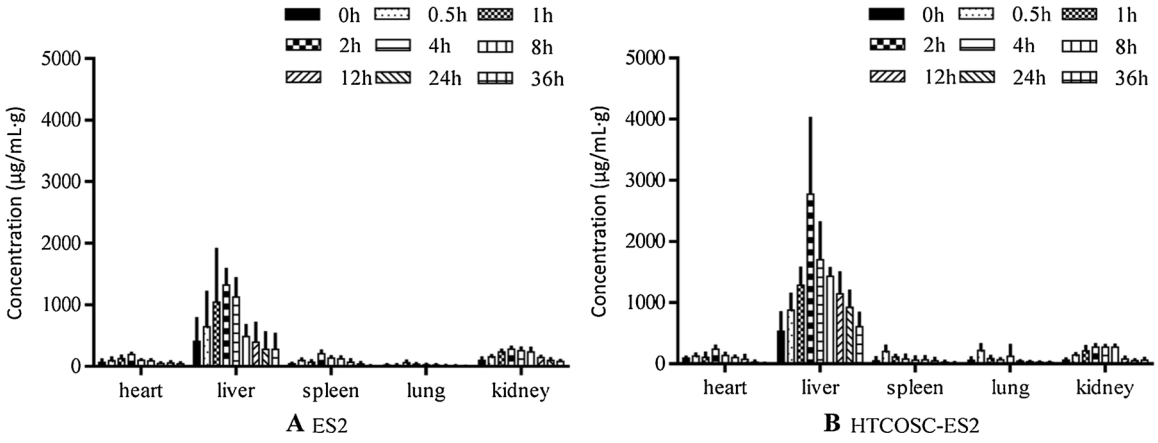


**Fig. 9.** Tissue distribution at different time points after single intravenous injection of ES2 and HTCOSC-ES2 in mice. Data are expressed as the mean ± SD, $n$ = 6.

effects of ES2 and HTCOSC-ES2 on related proteins *in vivo* using immunohistochemistry.

The anti-angiogenic effects of endostatin are related to VEGF activity. Besides blocking VEGF-induced tyrosine phosphorylation of KDR/Flk-1, endostatin also can downregulates VEGF expression (Folkman, 2006b; Lin et al., 2017). In this study, the expression of VEGF decreased in the ES2 and HTCOSC-ES2 groups, compared to that in the NaCl group, and it was lower in the HTCOSC-ES2 group than in the ES2 group. Therefore, results indicated that ES2 and HTCOSC-ES2 could inhibit the expression of VEGF in tumor tissues.

Vascular proliferation in tumor tissue reflects the ability of the tumor to induce angiogenesis; therefore, MVD can be used as an indicator of tumor angiogenesis (Deliu et al., 2016). MVD was significantly reduced in the HTCOSC-ES2 group, compared to that in the ES2 group. We found that both ES2 and HTCOSC-ES2 inhibited cell cycle progression and arrested the endothelial cells in the $G_0$-$G_1$ phase *in vitro*. Additionally, *in vivo* experiments showed that ES2 and HTCOSC-ES2 inhibited tumor angiogenesis, thereby inhibiting tumor growth.

Endostatin was shown to induce apoptosis in HUVECs by activating caspase-3 and decreasing Bcl-2/Bax ratio. Chitooligosaccharides can also induce apoptosis of tumor cells by increasing the expression of caspase-3. *In vitro* experiments showed that the mixture group was inferior to the HTCOSC-ES2 group in inhibiting cell growth and promoting apoptosis, whereas conjugation enhanced the activity of both ES2 and HTCOSC. Therefore, in the HTCOSC-ES2 group, the number of MVD was less than that in the ES2 group, whereas the expression of caspase-3 was higher than that in the ES2 group. In conclusion, tumor inhibition experiments and immunohistochemical assays showed that both ES2 and HTCOSC-ES2 could inhibit the growth of endothelial cells and promote cell apoptosis. However, HTCOSC-ES2 showed higher activity than ES2.

In the pharmacokinetic study, the half-life of HTCOSC-ES2 was significantly prolonged, and its bioavailability was improved after single intravenous administration to mice, compared to those of ES2. Regarding tissue distribution, ES2 and HTCOSC-ES2 were mainly distributed in the liver and kidneys. In the liver, both ES2 and HTCOSC-ES2 reached a maximum concentration at 2 h. However, HTCOSC-ES2 concentration in the liver was higher than that of ES2, indicating that HTCOSC-ES2 exhibited liver targeting. In addition, HTCOSC-ES2 was distributed in the lungs, whereas its concentration in other tissues was very low. These results indicated that HTCOSC-ES2 exhibited greater liver targeting than ES2.

## 5. Conclusions

In this study, we conjugated ES2 to a soluble chitooligosaccharide (HTCOSC) to form a HTCOSC-ES2 polymer. Our results showed that ES2 and HTCOSC-ES2 were mainly taken up by endothelial cells through the clathrin and lipid-valve pathways and transported to the nucleus, which arrested the cells in the $G_0/G_1$ phase, thereby inhibiting the proliferation of endothelial cells. Although both ES2 and HTCOSC could increase caspase-3 expression and promote apoptosis, the proapoptotic effects of HTCOSC-ES2 *in vivo* were stronger, resulting in a decrease in the number of microvessels in the tumor and effective suppression of tumor growth. The positive charge of HTCOSC-ES2 prolonged its uptake time by the endothelial cells, increased its half-life, and resulted in liver targeting, which prolonged its duration of action in the liver and reduced its clearance. This study showed that although both ES2 and HTCOSC-ES2 exhibited anti-angiogenic effects, promoted apoptosis, and inhibited tumor growth *in vitro* and *in vivo*, HTCOSC-ES2 might have a higher potential for the treatment of angiogenesis-related diseases. Therefore, HTCOSC-ES2 might be a candidate anticancer drug.

## Conflict of interest

The authors have no conflicts of interest.

## Author contributions

Zhendong Wang and Haining Tan designed the research and prepared the manuscript. Liang Xing and Yan Li participated in the overall experiments. Feng Sun and Zhifang Yang participated in analyzing the data. Fengshan Wang discussed the results.

## Acknowledgments

This work was supported by National Natural Science Foundation of China (81473129), Shandong Provincial Key Research and Development Program (2015GSF118099), Shandong Provincial Natural Science Foundation (ZR2015HM043) and the Fundamental Research Funds of Shandong University (2014JC044).

## References

Li, Jia, L., Guo, L. F., Yu, M., Sun, X., Nie, W., & Luo, Y. Z. (2015a). Pharmacokinetics of PEGylated recombinant human endostatin (M2ES) in rats. *Acta Pharmacologica Sinica, 36*(7), 847–854.

Li, Z., Yuan, Z.-F., Mu, G.-Y., Hu, M., Cao, L.-J., Zhang, Y.-L., ... Ge, M.-X. (2015b). Augmented anti-angiogenesis activity of polysulfated heparin-endostatin and polyethylene glycol-endostatin in alkali burn-induced corneal ulcers in rabbits. *Experimental and Therapeutic Medicine, 10*(3), 889–894.

Casal, E., Federici, L., Zhang, W., Fernandez Recio, J., Priego, E. M., Miguel, R. N., ... Laue, E. D. (2006). The crystal structure of the BAR domain from human Bin1/amphiphysin II and its implications for molecular recognition. *Biochemistry, 45*(43), 12917–12928.

Chen, Chen, Y. C., Du, Y., Han, Z., Ying, H., Bouchard, R. R., & Hung, M. C. (2017). A tumor vessel-targeting fusion protein elicits a chemotherapeutic bystander effect in pancreatic ductal adenocarcinoma. *American Journal of Cancer Research, 7*(3), 657–672.

Chen, Wang, S., Lu, X., Zhang, H., Fu, Y., & Luo, Y. (2011). Cholesterol sequestration by nystatin enhances the uptake and activity of endostatin in endothelium via regulating distinct endocytic pathways. *Blood, 117*(23), 6392–6403.

Deliu, I. C., Neagoe, C. D., Bezna, M., Genunche Dumitrescu, A. V., Toma, S. C., Ungureanu, B. S., & ForTofoiu, M. (2016). Correlations between endothelial cell markers CD31, CD34 and CD105 in colorectal carcinoma. *Romanian Journal of Morphology and Embryology, 57*(3), 1025–1030.

Dhanabal, M., Ramchandran, R., Waterman, M. J. F., Lu, H., Knebelmann, B., Segal, M., ... Sukhatme, V. P. (1999). Endostatin induces endothelial cell apoptosis. *The Journal of Biological Chemistry, 274*(17), 11721–11726.

Ding, R. L., Xie, F., Hu, Y., Fu, S. Z., Wu, J. B., Fan, J., ... Wen, Q. (2017). Preparation of endostatin-loaded chitosan nanoparticles and evaluation of the antitumor effect of such nanoparticles on the Lewis lung cancer model. *Drug Delivery, 24*(1), 300–308.

Edebali, N., Tekin, I. O., Acikgoz, B., Acikgoz, S., Barut, F., Sevinc, N., ... Sumbuloglu, V. (2014). Apoptosis and necrosis in the circumventricular organs after experimental subarachnoid hemorrhage as detected with annexin V and caspase 3 immunostaining. *Neurological Research, 36*(12), 1114–1120.

Enari, M., Sakahira, H., Yokoyama, H., Okawa, K., Iwamatsu, A., & Nagata, S. (1998). A caspase-activated DNase that degrades DNA during apoptosis, and its inhibitor ICAD. *Nature, 391*(6662), 43–50.

Farsad, K., Ringstad, N., Takei, K., Floyd, S. R., Rose, K., & De Camilli, P. (2001). Generation of high curvature membranes mediated by direct endophilin bilayer interactions. *The Journal of Cell Biology, 155*(2), 193–200.

Folkman, J. (1972). Anti-angiogenesis: New concept for therapy of solid tumors. *Annals of Surgery, 175*(3), 409–416.

Folkman, J. (2006a). Antiangiogenesis in cancer therapy–endostatin and its mechanisms of action. *Experimental Cell Research, 312*(5), 594–607.

Folkman, J. (2006b). Antiangiogenesis in cancer therapy—Endostatin and its mechanisms of action. *Experimental Cell Research, 312*(5), 594–607.

Gianni Barrera, R., Trani, M., Fontanellaz, C., Heberer, M., Djonov, V., Hlushchuk, R., & Banfi, A. (2012). VEGF over-expression in skeletal muscle induces angiogenesis by intussusception rather than sprouting. *Angiogenesis, 16*(1), 123–136.

Gong, Y. F., Zhang, X. M., Liu, F., Wang, Z. Z., Deng, X. F., Jiao, Y., ... Huang, X. Y. (2016). Inhibitory effect of recombinant human endostatin on the proliferation of hypertrophic scar fibroblasts in a rabbit ear model. *European Journal of Pharmacology, 791*, 647–654.

Hanai, J., Dhanabal, M., Karumanchi, S. A., Albanese, C., Waterman, M., Chan, B., ... Sukhatme, V. P. (2002). Endostatin causes G1 arrest of endothelial cells through inhibition of cyclin D1. *The Journal of Biological Chemistry, 277*(19), 16464–16469.

He, G., Xue, G., Xiao, L., Wu, J. X., Xu, B. L., Huang, J. L., ... Huang, W. L. (2005). Dynamic distribution and expression in vivo of human endostatin gene delivered by adenoviral vector. *Life Sciences, 77*(12), 1331–1340.

He, L., Zhao, C., Li, Y., Du, G., Liu, K., Cui, D., ... Chen, H. (2017). Antiangiogenic effects

of recombinant human endostatin in lung cancers. *Molecular Medicine Reports*.
Hosseini, H., Rajabibazl, M., Ebrahimizadeh, W., & Dehbidi, G. R. (2015). Inhibiting angiogenesis with human single-chain variable fragment antibody targeting VEGF. *Microvascular Research, 97*, 13–18.
Inamura, K. (2018). Update on immunohistochemistry for the diagnosis of lung Cancer. *Cancers, 10*(3).
Ishimoto, N., Nemoto, T., Nagayoshi, K., Yamashita, F., & Hashida, M. (2006). Improved anti-oxidant activity of superoxide dismutase by direct chemical modification. *Journal of Controlled Release, 111*(1-2), 204–211.
Jia, L. J., Xu, H. M., Ma, D. Y., Hu, Q. G., Huang, X. F., Jiang, W. H., ... Hua, Z. C. (2005). Enhanced therapeutic effect by combination of tumor-targeting Salmonella and endostatin in murine melanoma model. *Cancer Biology & Therapy, 4*(8), 840–845.
Jin, S., Zhang, Y., Yi, F., & Li, P. L. (2008). Critical role of lipid raft redox signaling platforms in endostatin-induced coronary endothelial dysfunction. *Arteriosclerosis, Thrombosis, and Vascular Biology, 28*(3), 485–490.
Karsan, A., Yee, E., Poirier, G. G., Zhou, P., Craig, R., & Harlan, J. M. (1997). Fibroblast growth factor-2 inhibits endothelial cell apoptosis by Bcl-2-dependent and independent mechanisms. *The American Journal of Pathology, 151*(6), 1775–1784.
Li, Liang, Y., Tang, Z. Y., Xiao, Y. N., Hao, H. P., & Wang, G. J. (2012). Quantification of endostar in rat plasma by LC–MS/MS and its application in a pharmacokinetic study. *Journal of Pharmaceutical and Biomedical Analysis, 70*, 505–511.
Li, Xing, R. E., Liu, S., & Li, P. C. (2016). Advances in preparation, analysis and biological activities of single chitooligosaccharides. *Carbohydrate Polymers, 139*, 178–190.
Liang, D.-S., Su, H.-T., Liu, Y.-J., Wang, A.-T., & Qi, X.-R. (2015). Tumor-specific penetrating peptides-functionalized hyaluronic acid- d -α-tocopheryl succinate based nanoparticles for multi-task delivery to invasive cancers. *Biomaterials, 71*, 11–23.
Lin, L., Chen, D., Xiang, Z. F., Pei, R. Z., Zhang, P. S., Liu, X. H., ... Lu, Y. (2017). Bortezomib could down-regulate the expression of RANKL, inhibit cell proliferation and induce cell apoptosis in the human myeloma cell line RPMI 8226 by activating casepase-3. *Cancer Biomarkers, 20*(2), 217–224.
Ling, Lu, N., Gao, Y., Chen, Y., Wang, S., Yang, Y., & Guo, Q. (2009). Endostar induces apoptotic effects in HUVECs through activation of caspase-3 and decrease of Bcl-2. *Anticancer Research, 29*(1), 411–417.
Ling, Y., Yang, Y., Lu, N., You, Q., Wang, S., Gao, Y., ... Guo, Q. L. (2007). Endostar, a novel recombinant human endostatin, exerts antiangiogenic effect via blocking VEGF-induced tyrosine phosphorylation of KDR/Flk-1 of endothelial cells. *Biochemical and Biophysical Research Communications, 361*(1), 79–84.
Liu, Huang, J., Sun, S., Zhou, Z., Zhang, J., Gao, F., & Sun, Q. (2015). Expression of matrix metalloproteinase-9, cyclooxygenase-2 and vascular endothelial growth factor are increased in gastrointestinal stromal tumors. *International Journal of Clinical and Experimental Medicine, 8*(4), 6495–6501.
Liu, J., Teng, L., Liu, C., Hu, L., Wang, Y., Liu, H., ... Wang, F. (2009). Augmented inhibitory effect of superoxide dismutase on superoxide anion release from macrophages by chemical modification with polysaccharide and attenuation effects on radiation-induced inflammatory cytokine expression in vitro. *Journal of Drug Targeting, 17*(3), 216–224.
Liu, L., Xin, Y., Liu, J., Zhang, E., & Li, W. (2017). Inhibitory effect of chitosan oligosaccharide on human hepatoma cells in vitro. *African Journal of Traditional Complementary and Alternative Medicines, 14*(4), 272–277.
Lu, X. Y., Ding, X. H., Zhong, L. J., Xia, H., Chen, X. D., & Huang, H. (2013). Expression and significance of VEGF and p53 in degenerate intervertebral disc tissue. *Asian Pacific Journal of Tropical Medicine, 6*(1), 79–81.
Ma, X., Yao, Y., Yuan, D., Liu, H., Wang, S., Zhou, C., ... Song, Y. (2012). Recombinant human endostatin endostar suppresses angiogenesis and lymphangiogenesis of malignant pleural effusion in mice. *PloS One, 7*(12), e53449.
Makinen, T., Veikkola, T., Mustjoki, S., Karpanen, T., Catimel, B., Nice, E. C., ... Alitalo, K. (2001). Isolated lymphatic endothelial cells transduce growth, survival and migratory signals via the VEGF-C/D receptor VEGFR-3. *The EMBO Journal, 20*(17), 4762–4773.
Mingming, Y., Yuanhong, W., Fugang, M., Weijie, Y., Tingfu, J., & Zhihua, L. V. (2017). Pharmacokinetics, tissue distribution and excretion study of fluoresceinlabeled PS916 in rats. *Current Pharmaceutical Biotechnology, 18*(5), 391–399.
Monteiro Amado, F., Castro, S., II, Lima, C. J., Soares, F. A., Kowalski, L. P., & Granjeiro, J. M. (2013). Immunohistochemical evaluation of MMP-2, MMP-9 and CD31/microvascular density in squamous cell carcinomas of the floor of the mouth. *Brazilian Dental Journal, 24*(1), 3–9.
O'Connor, D. S., Schechner, J. S., Adida, C., Mesri, M., Rothermel, A. L., Li, F., ... Altieri, D. C. (2000). Control of apoptosis during angiogenesis by survivin expression in endothelial cells. *The American Journal of Pathology, 156*(2), 393–398.
Ong, S. H., Jin, X. C., Jayasooriah, & Sinniah, R. (1996). Image analysis of tissue sections. *Computers in Biology and Medicine, 26*(3), 269–279.
Pu, C., Xu, H., Hu, J., Zheng, H., Huang, X., Zhang, C., ... Li, Y. (2012). RGD-modified endostatin fragments showed an antitumor effect through antiangiogenesis. *Anti-Cancer Drugs, 23*(8), 788–802.
Qiu, Z., Hu, J., Xu, H., Wang, W., Nie, C., & Wang, X. (2013). Generation of antitumor peptides by connection of matrix metalloproteinase-9 peptide inhibitor to an endostatin fragment. *Anti-Cancer Drugs, 24*(7), 677–689.
Shi, H., Xie, H., Zhao, Y., Lin, C., Cui, F., Pan, Y., ... Jiang, L. (2016). Myoprotective effects of bFGF on skeletal muscle injury in pressure-related deep tissue injury in rats. *Burns & Trauma, 4*, 26.
Sun, F., Yu, Y., Yang, Z., Wang, Z., Li, Y., Wang, F., ... Tan, H. (2018). Hyaluronic acid-endostatin2-alft1 (HA-ES2-AF) nanoparticle-like conjugate for the target treatment of diseases. *Journal of Controlled Release, 288*, 1–13.
Takei, K., Slepnev, V. I., Haucke, V., & De Camilli, P. (1999). Functional partnership between amphiphysin and dynamin in clathrin-mediatedendocytosis. *Nature Cell Biology, 1*(1), 33–39.
Talib, W. H., & Saleh, S. (2015). Propionibacterium acnes augments antitumor, anti-angiogenesis and immunomodulatory effects of melatonin on breast cancer Implanted in mice. *PloS One, 10*(4), e0124384.
Tjin, R. M., Sjin, T., Satchi Fainaro, R., Birsner, A. E., Ramanujam, V. M. S., Folkman, J., ... Javaherian, K. (2005). A 27-amino-acid synthetic peptide corresponding to the NH2-terminal zinc-binding domain of endostatin is responsible for its antitumor activity. *Cancer Research, 65*(9), 3656–3663.
Wan, A., Xu, Q., Sun, Y., & Li, H. (2013). Antioxidant activity of high molecular weight chitosan and N,O-ouaternized chitosans. *Journal of Agricultural and Food Chemistry, 61*(28), 6921–6928.
Wang, L. H., Rothberg, K. G., & Anderson, R. G. (1993). Mis-assembly of clathrin lattices on endosomes reveals a regulatory switch for coated pit formation. *The Journal of Cell Biology, 123*(5), 1107–1117.
Weidner, N. (1995). Intratumor microvessel density as a prognostic factor in cancer. *The American Journal of Pathology, 147*(1), 9–19.
Wickstrom, S. A., Alitalo, K., & Keski Oja, J. (2004). An endostatin-derived peptide interacts with integrins and regulates actin cytoskeleton and migration of endothelial cells. *The Journal of Biological Chemistry, 279*(19), 20178–20185.
Xu, L., Ji, X., Zhao, N., Song, C., Wang, F., & Liu, C. (2016). The conjugation of Cu/Zn superoxide dismutase (SOD) to O-(2-hydroxyl) propyl-3-trimethyl ammonium chitosan chloride (O-HTCC) enhances its therapeutic potential against radiation-induced oxidative damage. *Polymer Chemistry, 7*(9), 1826–1835.
Yu, Y., Sun, F., Zhang, C., Wang, Z., Liu, J., & Tan, H. (2016). Study on glyco-modification of endostatin-derived synthetic peptide endostatin2 (ES2) by soluble chitooligosaccharide. *Carbohydrate Polymers, 154*, 204–213.
Zhang, A. Y., Yi, F., Zhang, G., Gulbins, E., & Li, P. L. (2006). Lipid raft clustering and redox signaling platform formation in coronary arterial endothelial cells. *Hypertension, 47*(1), 74–80.
Zhao, N., Feng, Z., Shao, M., Cao, J., Wang, F., & Liu, C. (2017). Stability profiles and therapeutic effect of Cu/Zn superoxide dismutase chemically coupled to O-quaternary chitosan derivatives against dextran sodium sulfate-induced colitis. *International Journal of Molecular Sciences, 18*(6).